Water Research X 27 (2025) 100358

Contents lists available at ScienceDirect

Water Research X

journal homepage: www.sciencedirect.com/journal/water-research-x

Customizing surface grafting and interlayer functionalization for PFOA separation in polyamide membranes

Mohsen Pilevar [a], Hesam Jafarian [a], Nima Behzadnia [a], Qiaoli Liang [b], Sanam Etemadi Maleki [a], Sadegh Aghapour Aktij [c,d], Mohtada Sadrzadeh [c], Leigh Terry [a], Mark Elliott [a,*], Mostafa Dadashi Firouzjaei [a,c,*]

[a] Department of Civil, Construction, and Environmental Engineering, University of Alabama, Tuscaloosa, AL, 35487, USA
[b] Department of Chemistry and Biochemistry, University of Alabama, Tuscaloosa, AL, 35487, USA
[c] Department of Mechanical Engineering, 10-241 Donadeo Innovation Center for Engineering, Advanced Water Research Lab (AWRL), University of Alberta, Edmonton, AB, T6G 1H9, Canada
[d] Department of Chemical & Materials Engineering, Donadeo Innovation Centre for Engineering, University of Alberta, Edmonton, AB T6G 1H9, Canada

ARTICLE INFO

Keywords:
PFAS
Wastewater treatment
Metal-organic framework (Ag-MOF)
Thin-film nanocomposite (TFN) membranes
Fouling
Nanofiltration

ABSTRACT

Emerging contaminants, such as per- and polyfluoroalkyl substances (PFAS), pose significant challenges to ensuring a clean drinking water supply. This study evaluates various fabrication techniques for incorporating silver-based metal-organic frameworks (Ag-MOFs) into polyamide (PA) nanofiltration (NF) membranes to enhance perfluorooctanoic acid (PFOA) separation and anti-fouling performance. Various characterizations, including scanning and transmission electron microscopy, carboxylic group density, molecular weight cut-off (MWCO) measurements, and zeta potential analyses revealed that each method imparts distinct physicochemical and morphological characteristics to the modified membranes. Among all fabricated membranes, the interlayered Ag-MOFs (UI-MOF) obtained the highest permeance (13.7 $Lm^{-2}h^{-1}bar^{-1}$) but the lowest PFOA rejection (88.9 %), likely due to its loose PA network with large MWCO (522 Da) and high carboxylic group density (82.0 sites/nm^2). In contrast, the dip-coating surface-grafted Ag-MOFs (DS-MOF) achieved the highest PFOA rejection (93.4 %), attributed to its narrow pores (average pore diameter of 10 $\AA \pm 0.06$). Additionally, all modified membranes showed superior anti-fouling performance (flux recovery ratio > 94.0 %) compared to the Blank PA membrane, likely due to the improved surface hydrophilicity of the modified membranes.

1. Introduction

Water scarcity is a global challenge that necessitates concentrated efforts to ensure access to clean drinking water (Wolkeba et al., 2024). The rapid population growth and industrialization have led to the emergence of new contaminants in water resources, further complicating efforts to provide safe and reliable drinking water (Kebede et al., 2024). Among these contaminants, per- and polyfluoroalkyl substances (PFAS) have become a significant concern due to their toxicity, bioaccumulation, and severe health risks, such as cardiovascular disease (Cui et al., 2022), kidney and testicular cancer (Chang et al., 2014), thyroid disease (Melzer et al., 2010), and ulcerative colitis (Steenland et al., 2013). Perfluorooctanoic acid (PFOA) and perfluorooctane sulfonate (PFOS) are two of the most widely used PFAS substances in industrial applications (Zhang et al., 2024). Recognizing their dangers, the United States (US) Environmental Protection Agency (EPA) has recently set stringent regulatory limits of 4 parts per trillion (ppt) for PFOA and PFOS ((EPA), U.S.E.P.A., 2024), emphasizing the urgent need for effective removal technologies.

Several technologies have been explored for PFAS removal and degradation, including thermal degradation (Sun et al., 2024; Longendyke et al., 2022), advanced oxidation (Zango et al., 2023), photocatalysis (Chen et al., 2021), adsorption (Ahn et al., 2022; Teng et al., 2024), and ion exchange (Liu and Sun, 2021; Woodard et al., 2017). However, these methods often suffer from high energy demands (Kucharzyk et al., 2017), slow treatment rates (Hopkins et al., 2018), and the risk of secondary pollution or transformation into shorter-chain PFAS structures (Merino et al., 2016). Pressure-driven filtration processes, such as nanofiltration (NF) and reverse osmosis (RO), offer a more efficient and cost-effective solution for PFAS removal, with NF

* Corresponding authors.
E-mail addresses: melliott@eng.ua.edu (M. Elliott), mdfirouzjaei@ua.edu (M. Dadashi Firouzjaei).

https://doi.org/10.1016/j.wroa.2025.100358
Received 3 March 2025; Received in revised form 22 May 2025; Accepted 26 May 2025
Available online 27 May 2025

often used as the pretreatment for RO processes (Mohammad et al., 2015). Among commercially available membranes, polyamide (PA) membranes are the most widely used in NF and RO systems due to their simple fabrication, durability, and affordability (Shao et al., 2022). However, membrane fouling, caused by organic and biological contaminants in wastewater, is a major challenge for PA membranes. Fouling can shorten the membrane lifespan, reduce the separation efficiency, and increase operational costs (Shao et al., 2022). Therefore, it is essential to address the anti-fouling properties when developing modified PA membranes, as susceptibility to fouling can undermine their long-term performance even in membranes demonstrating high PFOA separation efficiency.

A promising strategy for improving anti-fouling and separation performance in NF membranes is the integration of nanomaterials into the PA layer, forming thin-film nanocomposite (TFN) membranes (Urper-Bayram et al., 2020). However, chemical incompatibility, nanoparticle (NP) agglomeration, uncontrolled release of NPs, and structural defects are some of the common challenges associated with the fabrication of TFN membranes, which can diminish their filtration performance (Cheng et al., 2019). Hence, it is essential to employ appropriate methodologies for nanomaterial synthesis and membrane fabrication to minimize such potential drawbacks. Among various nanomaterials, metal-organic frameworks (MOFs) stand out as great candidates because of their large surface area, structural stability, uniform active metal site distribution, antibacterial properties, and strong compatibility with the PA layer (Zirehpour et al., 2016; Shah et al., 2024; Jafarian et al., 2023).

Our previous work revealed the potential of Ag-MOFs for mitigating biological fouling in TFN membranes through various integration techniques, including in-situ ultrasonication (Pilevar et al., 2024). Building on these findings, this study aims to **(1)** investigate how in-situ ultrasonication and dip-coating methods influence the physicochemical and structural properties of Ag-MOF-modified TFN membranes, **(2)** evaluate the PFOA separation performance of these membranes and

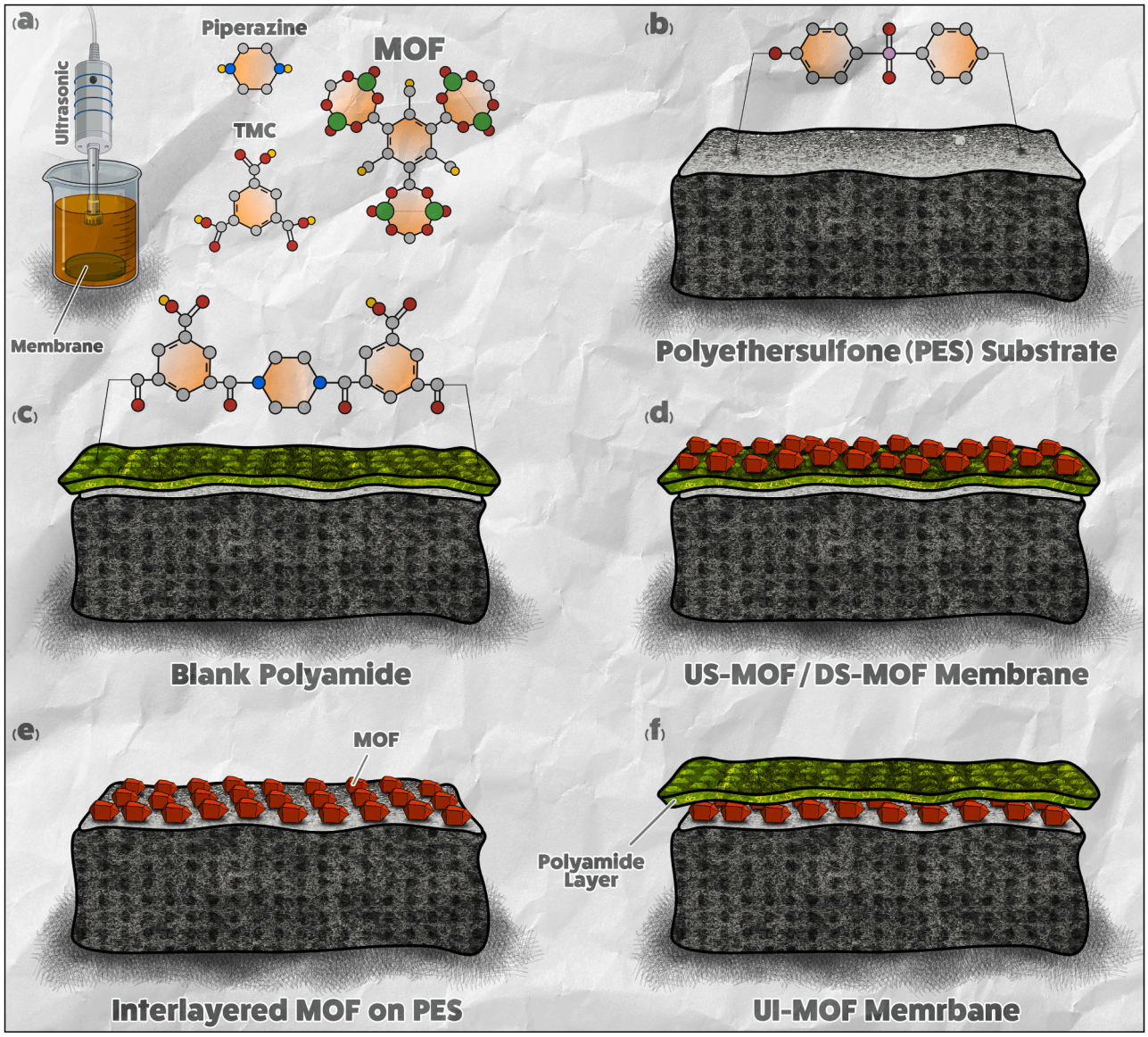

Fig. 1. Schematic illustration of **(a)** In-situ synthesis and growth of MOFs on the surface of the membrane, the chemical structure of piperazine and trimesoyl chloride (TMC) molecules used for the preparation of polyamide (PA) layer, and molecular structure of synthesized MOFs, **(b)** Chemical structure of PES support, **(c)** A PA layer fabricated on top of the PES support (i.e., Blank Membrane), **(d)** Schematic of surface-grafted MOFs on top of the Blank membrane (i.e., US-MOF and DS-MOF membranes), **(e)** Interlayered Ag-MOFs on top of the PES support before interfacial polymerization (IP) reaction, and **(f)** Schematic of interlayered MOFs beneath the PA layer (i.e., UI-MOF membrane).

their tunability for treating diverse wastewater streams, and **(3)** thoroughly examine their stability and antifouling properties for long-term use in potential field applications. The stability, PFOA separation, and anti-fouling performance of unmodified (Blank) and modified membranes were assessed in a crossflow NF system using various salts, PFOA, bovine serum albumin (BSA), and real lake water samples.

2. Results and discussion

2.1. Structural and morphological characteristics of membranes

Each integration technique can influence Ag-MOFs' positioning within the membrane structure (Fig. 1), leading to distinct physicochemical, structural, and morphological properties. The modified PA membranes were prepared by integrating the synthesized Ag-MOFs (**Figure S1**) via interlayering and surface-grafting assembly techniques. The ultrasonically interlayered and surface-grafted Ag-MOF were labeled UI-MOF and US-MOF, respectively. The modified membrane with dip-coated surface-grafted Ag-MOFs was also labeled DS-MOF (Table 1). The selective PA layer of all membranes was fabricated via an interfacial polymerization reaction using piperazine (PIP) and trimesic chloride (TMC) as monomers (Pilevar et al., 2024).

Top-surface SEM and cross-section TEM imaging techniques were utilized to assess the structural and morphological characteristics of Blank and modified membranes (Fig. 2). Top-surface SEM images demonstrate that Ag-MOFs were successfully embedded within the PA networks of the modified membranes. Notably, the visible presence of Ag-MOFs on the surface-grafted membranes highlights the effectiveness of the employed integration techniques. Energy Dispersive X-ray (SEM-EDX) mapping analyses (**Table S1**) further confirmed the presence of Ag atoms within the structure of the modified membranes. The structural variation between the PA layers of the fabricated membranes highlights the crucial effects of Ag-MOFs and their integration techniques on the morphological and surface characteristics of the modified membranes. For instance, the unique nodular patterns of PA layer morphology in the US-MOF membrane are known to elevate the surface roughness in TFN membranes (Shao et al., 2022). This is consistent with the average surface roughness of the US-MOF membrane (Table 2), which was the highest (65.9 nm) among all fabricated membranes. The cross-section TEM images of the modified membranes were obtained to confirm the integration of Ag-MOFs within and underneath the active PA layer. The apparent contrast between the PES support, PA active layer, and Ag-MOFs confirms the effectiveness of the applied incorporation methods.

The surface roughness and hydrophilicity of the fabricated membranes were further assessed via AFM (Fig. 2) and water contact angle measurements, respectively. Ag-MOF integration into the membrane structure improved surface hydrophilicity by reducing the water contact angles in all modified membranes (Table 2). This can be due to the intrinsic hydrophilic functional groups of Ag-MOFs (Firouzjaei et al., 2018), particularly in surface-grafted membranes where Ag-MOFs are predominantly distributed on the membrane surface. Additionally, it is important to note that each integration method imparts distinct surface chemistries to the modified membranes, which can influence their surface hydrophilicity, as further discussed in the following section on carboxylic group densities. The elevated surface hydrophilicity can promote surface wettability, water permeability, and fouling mitigation in the modified membranes. The surface roughness properties of Blank and modified membranes varied significantly (Table 2), with the UI-MOF membrane showing the lowest (40.8 nm) average surface roughness.

Table 1
Description of Blank and modified PA membranes used in this study and the techniques employed to integrate Ag-MOFs into their structure.

Membrane	Preparation Description
Blank	Blank polyamide (PA) membrane (without Ag-MOFs)
UI-MOF	Ag-MOFs were interlayered on top of polyethersulfone (PES) support (via ultrasonication) before the IP reaction.
US-MOF	Ag-MOFs were ultrasonically synthesized and surface-grafted on top of the Blank PA membrane.
DS-MOF	Ag-MOFs were surface-grafted on top of the Blank PA membrane via the dip-coating technique.

2.2. Physicochemical and ion transport properties of membranes

The physicochemical properties and elemental compositions of the Blank and modified membranes were investigated using XPS and EDX analyses. The deconvoluted high-resolution spectra for O 1s, N 1s, C 1s, and Ag 3d were obtained to analyze the XPS results (**Figure S2-S5**). The prominent peaks at 530, 400, and 285 eV correspond to O 1s, N 1s, and C 1s elemental signals, respectively (Xie and Sherwood, 1992; Khorshidi et al., 2015). The peaks associated with Ag $3d_{5/2}$ (368 eV) and Ag $3d_{3/2}$ (373 eV) were also detected in the XPS spectra of the modified membranes (Firouzjaei et al., 2018; Park et al., 2016). Additionally, Ag atoms were detected in the EDX spectra of all modified membranes (**Table S1**), further confirming the effectiveness of the applied integration techniques. Moreover, Specific binding energies were used to identify different chemical bonds and functional groups within Blank and modified membranes (**Tables S2-S4**).

The ion transport properties of PA membranes can provide crucial information about the mechanisms governing their permselectivity. For instance, stream potential analysis (zeta potential measurements) can provide valuable insight into the surface charge characteristics of TFN membranes, enabling the assessment of their electrostatic interactions with charged solutes in water. All fabricated membranes showed negative zeta potential across the pH range of 4 to 9 (Fig. 3**a**), while the DS-MOF membrane exhibited a slightly more negative value (−26.50 mV) at a pH of 7, underscoring its potential for effective electrostatic repulsion of negatively charged solutes like PFOA.

The molecular weight cut-off (MWCO) measurements were also conducted to assess the size exclusion capabilities of Blank and modified membranes (Fig. 3**b**). The MWCO refers to the smallest molecular weight (in Daltons) at which the membrane achieves a 90 % rejection for a neutral solute (e.g., polyethylene glycol (PEG)) with a known molecular weight. The measured MWCO values (Da) were further used to estimate the average pore size diameter (d_p) of the membranes resulting in the sequence: UI-MOF>US-MOF>Blank>DS-MOF, with UI-MOF and DS-MOF membranes obtaining pore sizes of 14 ± 0.1 and 10 $\AA$ ± 0.1, respectively. The larger pores obtained by the UI-MOF membrane can be due to the lower PA cross-linking degree because of the high interlayer MOF loading on the PES support (Liu et al., 2022). Generally, the size exclusion capabilities of NF membranes improve as the average pore size decreases (Boo et al., 2018), which shows the great potential of DS-MOF membranes for size exclusion of small solutes.

Additional mixed salt filtration experiments were conducted using a highly concentrated mixture of salts (containing 250 mg/L NaCl, Na_2SO_4, $CaCl_2$, and $MgSO_4$) with an ionic strength of 97 mM to further assess the roles of steric hindrance and electrostatic exclusion in the overall selectivity of Blank and modified membranes under dynamic conditions. Feed solutions with such high ionic strength can screen the surface potential of the membrane, enabling a more precise evaluation of the separation mechanisms of NF membranes (Boo et al., 2018). Notably, the DS-MOF membrane showed superior rejection performance for all individual ions (Fig. 3**c**), highlighting their strong potential for steric exclusion of small solutes as the electrostatic exclusion was greatly reduced. In addition, the significant decline in the rejection of Na^+ ions by the UI-MOF membrane indicates that electrostatic exclusion plays a crucial role in the overall selectivity of the UI-MOF membrane.

The carboxylic group density of the Blank and modified membranes was measured to further assess their physicochemical properties. Carboxyl groups, located on the membrane surface and within the pores,

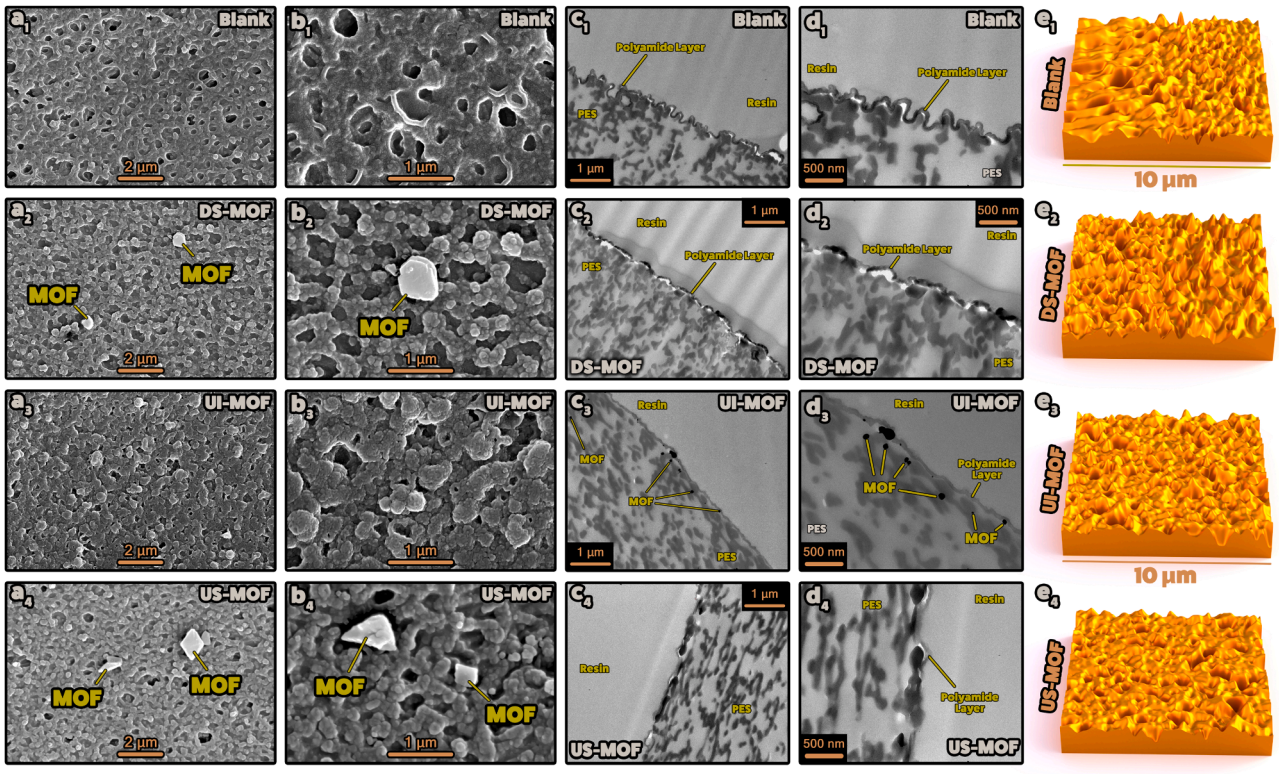

Fig. 2. Morphological and surface characteristics of membranes are illustrated through low and high magnification top surface SEM, cross-sectional TEM images, and surface roughness diagrams of ($\mathbf{a_1}$-$\mathbf{d_1}$) Blank, ($\mathbf{a_2}$-$\mathbf{d_2}$) DS-MOF, ($\mathbf{a_3}$-$\mathbf{d_3}$) UI-MOF, and ($\mathbf{a_4}$-$\mathbf{d_4}$) US-MOF. AFM results were used to prepare schematics of membranes' surface roughness ($\mathbf{e_1}$-$\mathbf{e_4}$). The top-surface SEM and cross-section TEM images confirm the presence of Ag-MOFs within the modified membranes. Moreover, SEM images highlight the morphological difference between the Blank and modified membranes, indicating the effect of various incorporation techniques on surface characteristics. These surface alterations highly influence the overall filtration performance of the modified membranes. Surface roughness images were made from the surface matrix coordinates of the membranes.

Table 2
Roughness and water contact angle values of the Blank modified PA membranes.

Membrane	Average Roughness (nm)	Root Mean Square Roughness (nm)	Water Contact Angle (°)	Zeta Potential at pH=7 (mV)
Blank	58.6	41.8	49.7	−23.82
UI-MOF	40.8	32.2	39.1	−23.57
US-MOF	65.9	48.7	42.7	−24.5
DS-MOF	58.1	44.0	42.9	−26.5

were measured using the ion elution method (Boo et al., 2018). Higher densities of carboxylic groups can bolster the formation of a hydration layer on the membrane surface via hydrogen bonding and ion-dipole interactions with water molecules, which can facilitate the transport of water molecules. Deprotonated carboxylic groups can also contribute to the retention rate of negatively charged solutes by enhancing the electrostatic rejection capabilities of NF membranes. The integration of Ag-MOFs increased the carboxylic group densities of all modified membranes, likely due to the additional carboxyl groups within the MOF structure (Fig. 3**d**). The elevated carboxylic group densities in the modified membranes may contribute to their enhanced surface hydrophilicity compared to the Blank membrane. Notably, ultrasonic-assisted integration of Ag-MOFs resulted in increased densities of the carboxylic groups within the UI-MOF (82.0 sites/nm^2) and US-MOF (59.5 sites/nm^2) compared to the Blank membrane (10.2 sites/nm^2). The high density observed in the UI-MOF (82.0 sites/nm^2) membrane likely plays a key role in its superior surface hydrophilicity compared to the other modified membranes.

2.3. Filtration and fouling performance

The water flux and PFOA rejection performance of Blank and modified membranes were evaluated through filtration tests performed in a crossflow system, utilizing feed solutions with 1 mg/L of PFOA in deionized (DI) water. All modified membranes obtained higher water permeance (Fig. 4**a**) than the Blank (8.5 Lm^{-2}h^{-1}bar^{-1}), which can be attributed to their improved surface hydrophilicity (Table 2). Notably, the UI-MOF membrane achieved the highest permeance (13.7 Lm^{-2}h^{-1}bar^{-1}), potentially due to the hydrophilic interactions between water molecules and the membrane surface, followed by facilitated water passage through the large pores (14 Å ± 0.1) of their selective layer. The observed water permeance of the Blank and modified membranes is further supported by their carboxylic group densities (Fig. 3**d**). Notably, UI-MOF and US-MOF membranes with the highest carboxylic group densities of 82.0 and 59.5 sites/nm^2 offered superior water permeance of 13.7 and 12.1 Lm^{-2}h^{-1}bar^{-1}, respectively. This can be due to the bolstered formation of a strong hydration layer as described earlier.

The PFOA rejection performance of the membranes (Fig. 4**a**) followed the order: DS-MOF>US-MOF>Blank>UI-MOF, with DS-MOF and US-MOF membranes slightly outperforming the Blank membrane by 1.1 % and 0.5 %, respectively. The membrane characteristics, PFOA properties, and feed solution quality are crucial factors in identifying the governing mechanisms (steric hindrance and/or electrostatic exclusion) in PFOA rejection by NF membranes. PFOA compounds are negatively charged molecules at neutral pH conditions with an average molecular weight (Mw) of 414 Da (Xiong et al., 2021). The negatively charged surfaces of Blank and modified membranes (Fig. 3**a**) highlight their potential for electrostatic exclusion of PFOA molecules, particularly in the DS-MOF membrane, because of its slightly more negative zeta

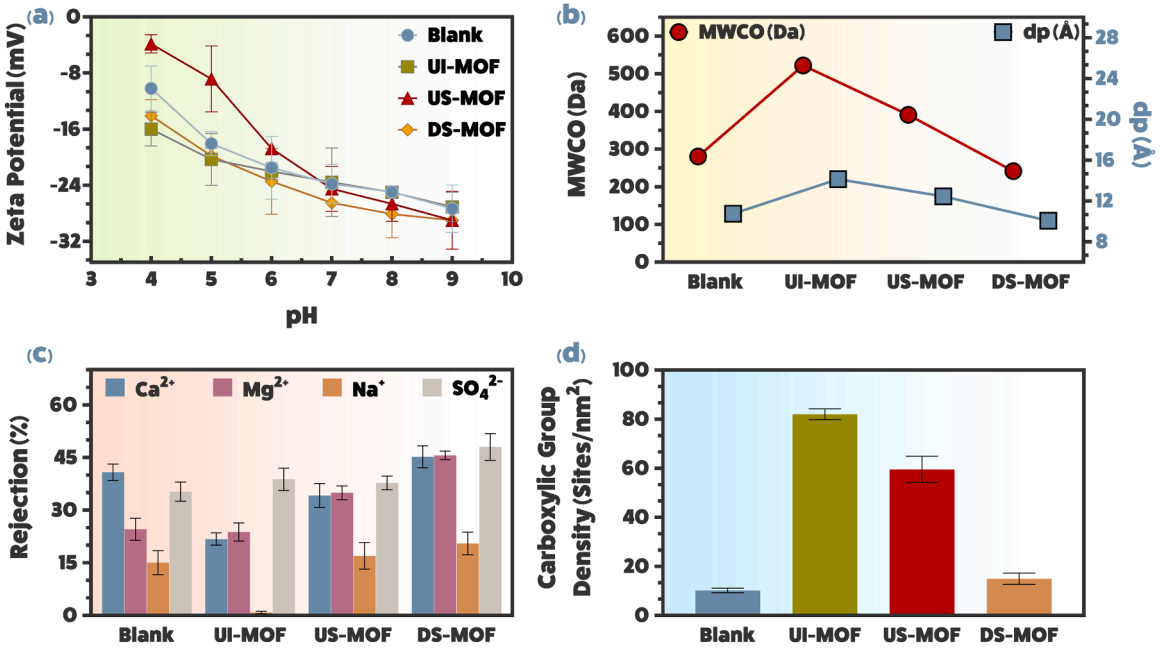

Fig. 3. **(a)** Zeta potential measurements at a pH range of 4–9, **(b)** Molecular weight cut-off (MWCO) and average pore diameter (d_p), **(c)** Individual ion rejection performance achieved by Blank and modified membranes during the mixed salt filtration test. **(d)** Carboxylic group density of the Blank and modified membranes. The MWCO and pore size diameter estimations underscore the steric hindrance capability of the membranes, with lower values suggesting greater solute size exclusion potentials. Notably, UI-MOF and DS-MOF membranes possess the highest and lowest MWCO values, respectively. The charge characteristics of Blank and modified membranes were assessed via the zeta potential measurements. The DS-MOF membranes possess the largest (negative) zeta potential, which can potentially boost their electrostatic rejection performance by forming a stronger electrostatic field on the surface of the membrane. The elevated carboxylic group densities in UI-MOF and US-MOF membranes highlight the influence of in-situ ultrasonic techniques on the surface chemistry of the modified membranes, which can potentially enhance their water permeance and electrostatic exclusion capabilities.

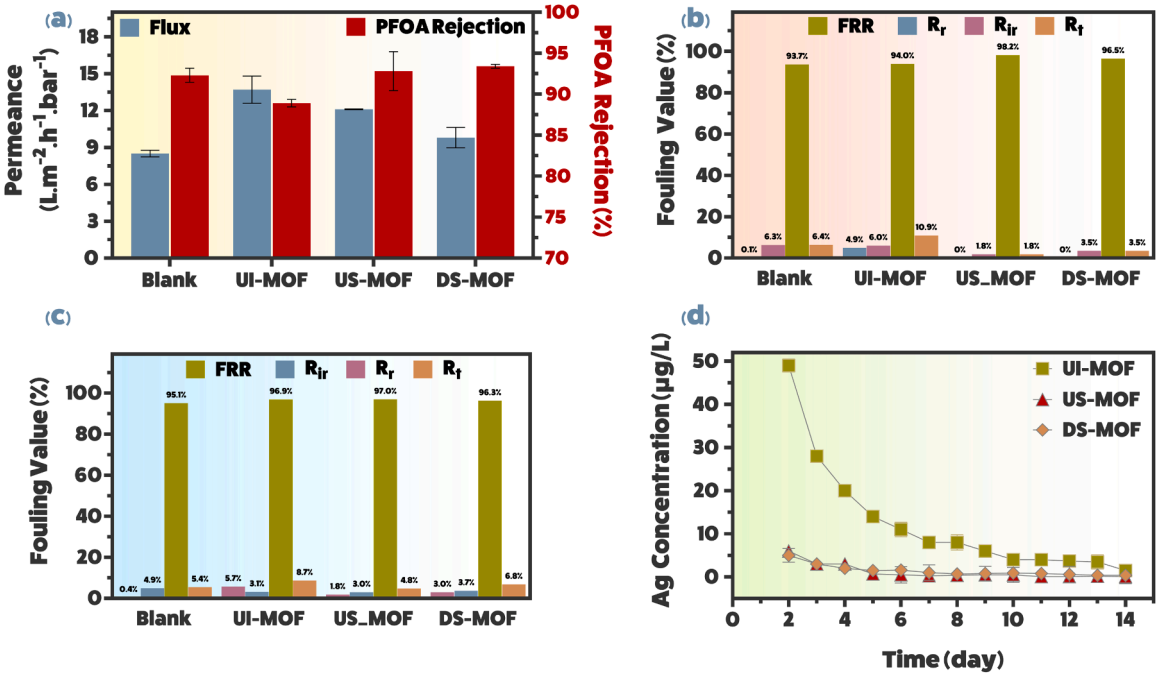

Fig. 4. **(a)** Filtration performance of the Blank and modified membranes, showing water flux and PFOA rejection, **(b)** Antifouling performance of the fabricated membranes with an aqueous feed solution comprised of DI water, Bovine serum albumin (BSA) (200 mg/L), and PFOA (1 mg/L), **(c)** Anti-fouling performance of the fabricated membranes with synthetic wastewater containing NaCl (950 mg/L), $CaCl_2$ (50 mg/L), and PFOA (1 mg/L), and **(d)** The concentration profile (13 consecutive days) of released silver ions from the modified membranes in a batch mode test. The UI-MOF membrane achieved the highest water flux and lowest PFOA rejection rate among all fabricated membranes, highlighting the critical role of their large MWCO (522 Da) compared to Blank and other modified membranes. Conversely, the US-MOF and DS-MOF membranes obtained higher PFOA rejection rates while offering superior anti-fouling and stability performances under long-term (96 h) filtration tests. The release of silver from all modified membranes remained under 100 µg/L, aligning with the maximum regulatory limit for silver.

potential (Table 2). However, the minimal difference between the PFOA rejection rates obtained by DS-MOF and other membranes suggests that electrostatic exclusion is not the sole mechanism for PFOA retention by the fabricated membranes. Steric hindrance also plays a crucial role, given the relatively high Mw of PFOA (414 Da) compared to the MWCO values of the fabricated membranes (Table 3). DS-MOF membrane possesses the smallest MWCO (242 Da) among all fabricated membranes, highlighting its great potential for size exclusion of PFOA molecules. Conversely, the UI-MOF membrane obtained the largest MWCO (522 Da), limiting its steric exclusion capabilities. As previously revealed by the mixed salt filtration results (Fig. 3**c**), the electrostatic exclusion mechanism plays a crucial role in solute retention by the UI-MOF membrane. This agrees with the relatively low PFOA rejection performance of the UI-MOF membrane (88.9 %). In contrast, the high PFOA rejection rate obtained by the DS-MOF membrane (93.4 %) agrees with its strong steric hindrance and electrostatic exclusion capabilities for the retention of negatively charged PFOA molecules.

Additional filtration tests were carried out to assess the anti-fouling properties of Blank and modified membranes when exposed to organic foulants such as BSA. All modified membranes achieved higher FRRs (%) than the Blank membrane (Fig. 4**b**), which is likely due to their enhanced surface hydrophilicity, as evidenced by their lower water contact angles compared to the Blank membrane (Table 2). In addition, the excellent anti-fouling performance of the US-MOF (FRR of 98.2 %) and DS-MOF (FRR of 96.5 %) membranes can be attributed to their highly negative surface charge (Table 2), which enhances electrostatic repulsion against negatively charged BSA molecules at neutral pH (Ang and Elimelech, 2007). Long-term stability and antifouling performance of the membranes were further evaluated through 7-day filtration tests using real surface water samples collected from the Black Warrior River, AL. As shown in **Figure S6**, the DS-MOF and UI-MOF membranes exhibited excellent stability and antifouling performance (FRR >90 %) under prolonged operational conditions, highlighting their potential for practical field applications.

Further filtration tests were conducted to evaluate the stability of the membranes by monitoring their water flux performance after long-term (96 h) exposure to complex feed solutions containing a mixture of salts (NaCl and $CaCl_2$) and PFOA compounds. All modified membranes achieved stable water fluxes (Fig. 4**c**) by outperforming the Blank membrane (FRR of 95.1 %). In contrast to anti-fouling results, both R_r and R_{ir} contributed to the total flux decline ratio (R_t) of Blank and modified membranes, with UI-MOF and US-MOF membranes showing the highest (8.7 %) and lowest (4.8 %) R_t values, respectively.

The potential release of silver ions into ecosystems can pose toxicity toward microorganisms, mammals, and aquatic life by disrupting cellular functions (Fabrega et al., 2011). The World Health Organization (WHO) has set 100 μg/L as the regulatory concentration limit for silver in drinking water (Organization, 2022). Hence, it was essential to measure the release of Ag^+ ions to ensure sustainability, environmental safety, and the chemical stability of Ag-MOF-modified membranes. Silver ion release from the modified membranes was assessed over a two-week batch experiment, where membrane coupons (2 cm^2) were immersed in fresh DI water, and the concentration of released Ag ions was measured daily. The UI-MOF membrane showed a sharp release profile during the first 4 days, which transitioned into a more stable and controlled release rate (Fig. 4**d**). Conversely, the US-MOF and DS-MOF membranes exhibited a more controlled and stable release over time. Notably, the Ag^+release levels of all modified membranes were below 100 μg/L, which complies with the maximum regulatory concentration of Ag. Overall, the stable filtration performance and controlled Ag^+ release from the modified membranes highlight their robustness for potential field applications in treating complex wastewater streams.

The perm-selectivity of the modified membranes (i.e., UI-MOF and DS-MOF) was further evaluated through filtration tests conducted at higher operating pressures ranging from 6 to 14 bar. As illustrated in **Figure S7**, operating at elevated pressures resulted in increased water flux and moderate declines (<15 %) in the rejection performance of the Blank and modified membranes. It is worth noting that all tested membranes maintained their structural stability under high operating pressures (14 bar), further highlighting their potential for field applications.

Compared to previously reported TFN membranes for PFOA removal (Table 3), the Ag-MOF-modified membranes developed in this study exhibit promising properties, such as strong antifouling performance and operational stability. Additionally, the membranes maintained low silver ion release levels ($\leq$ 50 μg/L) while delivering stable filtration performance under extended operation with real lake water samples, demonstrating their potential for field applications. The applied integration techniques also enabled tunable MWCO values ranging from 242 to 522 Da, allowing the membranes to be tailored for treating complex wastewater streams.

2.4. *Comparison of fabricated membranes and recommendation of the best membrane*

The three modified membranes, UI-MOF (ultrasonically interlayered Ag-MOF), US-MOF (ultrasonically surface-grafted Ag-MOF), and DS-MOF (dip-coated surface-grafted Ag-MOF), demonstrated distinct physicochemical and separation properties. Their filtration performance was assessed and compared based on key factors including water

Table 3
Summary of other modified NF membranes and their PFOA rejection performance.

Membrane Type	MWCO (Da)/ Pore Diameter (Å)	Permeance ($Lm^{-2}h^{-1}bar^{-1}$)	PFOA Rejection (%)	PFOA Concentration (μg/L)	Ref
β-CDA/MMCNF[a]	346 Da	~9	~99.9	45–500	(Chaudhary et al., 2023)
Alginate NF[b]	324 Da	7.23	95.24	1000	(Tian et al., 2024)
Polyamide NF	12.2 Å	~11.6	90	1000	(Boo et al., 2018)
NF270 (commercial)	300 Da	-	99.1	100	(Sun et al., 2025)
PEM NF[c]	180 Da	16.1	~90	1000	(Wang et al., 2020)
SiO_2 /CMWCNT/PMIA[d]	661 Da	-	95.3–98.3	25–100	(Tang et al., 2022)
PNIPAm-PVDF[e]	8.8 Å	~14.2	~70	70	(Léniz-Pizarro et al., 2022)
NF90 (commercial)	7.2 Å	-	97.4	100	(Li et al., 2021)
UI-MOF	522 Da	13.7	88.9	1000	This work
US-MOF	391 Da	12.1	92.8		
DS-MOF	242 Da	9.8	93.4		
Blank	281 Da	8.5	91.6		

[a] β-cyclodextrin integrated Mixed-Matrix Composite Nano Filtration.
[b] Polyamide membrane with an interlayer of Sodium Alginate.
[c] Polyelectrolyte Multilayer Nano Filtration membrane.
[d] SiO_2 / Carboxylic Multiwalled Carbon Nanotube / Poly (m-phenylene isophthalamide).
[e] poly-N-isopropylacrylamide - Polyvinylidene fluoride.

permeance, PFOA rejection, antifouling, and stability (ion release).

(i) **Water Permeance:** All modified membranes outperformed the Blank membrane. UI-MOF exhibited the highest water permeance at 13.7 $Lm^{-2}h^{-1}bar^{-1}$, potentially attributed to its high carboxylic group density (82.0 sites/nm^2), large MWCO (522 Da), and loose PA network, facilitating water transport. US-MOF achieved moderate water permeance of 12.1 $Lm^{-2}h^{-1}bar^{-1}$, benefiting from increased hydrophilicity and carboxyl-rich Ag-MOFs. DS-MOF had the lowest water permeance at 9.8 $Lm^{-2}h^{-1}bar^{-1}$, which correlates with its tighter PA network and smaller pore size (242 Da MWCO).

(ii) **PFOA Rejection:** DS-MOF achieved the highest PFOA rejection, reaching 93.4 %, due to its narrow pore structure and strongest electrostatic repulsion. US-MOF followed closely with a rejection rate of 92.8 %, balancing steric and electrostatic exclusion. UI-MOF exhibited the lowest rejection at 88.9 %, as its looser structure relied primarily on electrostatic exclusion rather than steric hindrance.

(iii) **Antifouling Performance:** All modified membranes showed improved anti-fouling properties compared to the Blank membrane, which can be due to their improved surface hydrophilicity. UI-MOF, despite its high water permeance, showed the lowest antifouling performance with an FRR of 94.0 %, likely due to its larger pores and reduced steric hindrance against foulants.

(iv) **Stability and Silver Release Rate:** DS-MOF and US-MOF exhibited a controlled and stable silver release profile, ensuring minimal toxicity risks. UI-MOF showed a sharp initial Ag^+ release before stabilizing, which may raise concerns over long-term performance stability. The silver release levels for all membranes remained below the WHO regulatory limit of 100 μg/L.

While the UI-MOF membrane achieved the highest water permeance, its lower PFOA rejection and higher silver release rate make it less desirable. The US-MOF membrane provided a good compromise, offering high antifouling resistance, stable filtration performance, and moderate PFOA rejection. However, the DS-MOF membrane stood out as the best option due to its superior PFOA rejection, relatively high water permeance, strong antifouling properties, and stable Ag^+ release, making it ideal for long-term water treatment applications.

3. Materials & methods

3.1. Membrane fabrication

A commercial PES microfiltration membrane was employed as the support for the preparation of Blank and modified PA membranes. The interfacial polymerization reaction (to form a selective PA layer) was conducted using 10 mL of an aqueous solution containing 2 wt. % PIP and 0.4 wt. % TEA, applied to the surface of PES support for 2 min. Then, a 10 mL solution of 0.1 wt. % TMC in n-hexane was poured onto the membrane surface and allowed to react for 30 s to complete the IP reaction. After forming the selective PA layer, the membrane was cured in an oven at 70 °C for 10 min to ensure complete polymerization.

The ultrasonically interlayered Ag-MOF membrane (labeled as UI-MOF) was fabricated through in-situ ultrasonication before IP. For this purpose, a PES support was mounted in a custom frame and placed at the bottom of a glass beaker (1 L), with an ultrasound probe positioned at a fixed distance (~15 mm) from the membrane surface to prevent damage. Ultrasonication was then implemented using 73.6 mM $AgNO_3$ and 59.4 mM BTC at 50 °C for 45 min. Afterward, the fabricated membrane was rinsed with deionized (DI) water to remove any visible nanoparticle clusters on the membrane surface. Finally, the IP reaction was performed on the PES support. The ultrasonically surface-grafted membrane (labeled as US-MOF) was fabricated using the same procedure using a Blank PA membrane instead of the PES support. No additional PA layer was synthesized on the surface of the US-MOF membrane after ultrasonication. The probe sonicator's operational settings were 500 W, 20 kHz frequency kHz, 40 % amplitude, and 5-second pulse pause time to fabricate both UI-MOF and US-MOF membranes.

Additionally, the surface-grafted Ag-MOF membrane via dip-coating (labeled as DS-MOF) was prepared by mounting a Blank PA membrane in a custom frame. Then, 10 mL of a 1 wt. % Ag-MOF solution, prepared from the synthesized Ag-MOFs and sonicated for 5 min, was poured onto the membrane surface and stirred for 1 h at 100 rpm. The fabricated membrane was then rinsed with DI water to remove any nanoparticle clusters on the membrane surface. All membranes used in this study were fabricated in sets of four and stored in DI water for up to three months before their use in PFOA separation and fouling filtration tests.

3.2. Filtration and fouling performance

The filtration performance of Blank and modified membranes was assessed using a crossflow filtration setup. Membranes were compacted (by DI water) at 8 bar for 15 h to reach a steady state water flux before the filtration tests. PFOA filtration experiments were conducted using 2.5 L of aqueous feed solutions, prepared by dissolving the required PFOA in DI water to obtain an initial PFOA concentration of 1 mg/L. 0.1 M HCl and $NaHCO_3$ solutions were used to adjust the pH of the feed solution (i.e., pH 7). Afterward, the operating pressure was set to 6 bar and kept constant throughout PFOA filtration tests. After 2 h of filtration, the permeate flux was measured using a digital scale (RC41M6, OHAUS, USA) and Eq. (1). (Nejad et al., 2022):

$$J_w = \frac{m}{A\Delta t} \tag{1}$$

where J_w (L m^{-2} h^{-1}; LMH) represents the water flux, m (kg) is the permeated water weight, A (m^2) denotes the membrane's active surface area, and Δt (h) is the operating time.

Feed and permeate samples were collected for further PFOA measurements (Supporting information) to calculate the rejection performance of Blank and modified membranes using Eq. (2) (Aktij et al., 2023):

$$R\ (\%) = 1 - \frac{C_p}{C_f} \times\ 100 \tag{2}$$

where C_p and C_f are PFOA concentrations (mg/L) of the permeate and feed, respectively. Eq. (2) was also used to calculate the individual ion rejection in mixed salt filtration experiments, conducted as described elsewhere (Pilevar et al., 2024). The chemical stability of the membranes was further evaluated through filtration tests conducted after pH-adjusted (using 0.1 M HNO_3 and NaOH solutions) treatment steps. Briefly explained, membranes were soaked (for 15 min) in 20 mL of pH-adjusted solutions under shaking conditions (100 rpm), followed by thorough rinsing with DI water before filtration tests. The filtration performance of the membranes was assessed by measuring water permeance and Na_2SO_4 rejection before and after the pH treatments, using a feed solution composed of DI water containing 1000 mg/L Na_2SO_4 salt.

The anti-fouling performance of membranes was investigated via long-term (96 h) filtration tests using BSA as the fouling agent. To achieve this, the filtration system was first sanitized with 50 % ethanol (v/v), followed by multiple washings with DI water. Then, the Blank membrane was compacted with DI water at 8 bar for 15 h. Then, the water flux was measured at 6 bar and recorded as J_{w0}. The operating pressure of all modified membranes was adjusted to obtain the same J_{w0} as the Blank membrane. Then, 96 h closed-loop filtration tests were carried out using an aqueous feed solution with initial BSA and PFOA concentrations of 200 mg/L and 1 mg/L, respectively. A feed solution pH of 7 was maintained throughout the filtration test. Water flux was measured at different time intervals, and the average of the measured water fluxes was recorded as J_{w1}. The feed solution was then replaced

with DI water (after 96 h), and the membrane was washed in the system by setting the operating pressure at 1 bar for 1 h. Afterward, the water flux of the cleaned membrane was measured and denoted as J_{w2}.

Similarly, a long-term (96 h) filtration test was conducted to evaluate the performance of Blank and modified membranes using synthetic wastewater containing 950 mg/L NaCl, 50 mg/L $CaCl_2$, and 1 mg/L PFOA as the feed solution. The flux measurements followed the same procedure as the PFOA/BSA fouling test. The anti-fouling performance of the membranes was further examined by carrying out long-term filtration tests (7 days) using actual surface water samples (as feed solution) collected from the Black Warrior River, which receives discharges from wastewater treatment plants (WWTPs). Multiple indices, namely the flux recovery ratio (FRR), reversible fouling resistance (R_r), irreversible fouling resistance (R_{ir}), and total flux decline ratio (R_t), were defined (Eq. (3)–(6)) and used to assess the anti-fouling and long-term performance of the membranes (Jafarian et al., 2023; Mazani et al., 2019):

$$FRR\ (\%) = \left(\frac{J_{w2}}{J_{w0}}\right) \times\ 100 \tag{3}$$

$$R_r\ (\%) = \left(\frac{J_{w2} - J_{w1}}{J_{w0}}\right) \times\ 100 \tag{4}$$

$$R_{ir}\ (\%) = \left(\frac{J_{w0} - J_{w2}}{J_{w0}}\right) \times\ 100 \tag{5}$$

$$R_t\ (\%) = R_r + R_{ir} = \left(\frac{J_{w0} - J_{w1}}{J_{w0}}\right) \times\ 100 \tag{6}$$

3.3. MWCO measurements

The steric hindrance properties of Blank and modified membranes were investigated via molecular weight cut-off (MWCO) measurements. Filtration experiments were conducted using a dead-end cell at an operating pressure of 4.8 bar. To achieve this, 200 mg/L feed solutions of polyethylene glycol (PEG) with molecular weights of 200, 300, 400, 600, and 1000 Da were prepared. The membranes were pre-compacted at 4.8 bar for 30 min to stabilize the water flux. Then, filtration tests commenced with the smallest molecular weight, PEG (200 Da), and the solution was continuously stirred to reduce concentration polarization. Samples from the feed, retentate, and permeate were collected for quantitative analysis by Matrix Assisted Laser Desorption Ionization Time of Flight Mass Spectrometry (MALDI-TOF MS). Between each test, membranes were cleaned by immersing them in deionized water and stirring at 200 rpm for 30 min to minimize any potential pore blockage caused by previously filtered PEG solutions. Rejection performance was calculated using Eq. (7) (Zhang et al., 2024) and plotted against the molecular weights of the PEG solutes. The average pore size diameter (d_p) of the membranes was also estimated using Eq. (8) (Sadrzadeh and Bhattacharjee, 2013):

$$R(\%) = \left(1 - \frac{C_p}{\left(\frac{C_F + C_R}{2}\right)}\right) \times\ 100 \tag{7}$$

$$d_p(nm) = 0.09\ (MWCO)^{0.44} \tag{8}$$

where C_p, C_F, and C_R are PEG concentrations (mg/L) of the permeate, feed, and retentate, respectively.

The MALDI-TOF MS experiments were performed on a Bruker rapifleX mass spectrometer equipped with a Bruker scanning smartbeam™ 3D laser of 355 nm wavelength (≥ 100 μJ/pulse). MALDI-TOF MS analysis was utilized to measure the concentration of PEG in samples by constructing calibration curves for each PEG (200, 300, 400, 600, and 1000 Da) at different concentration levels (in the range of 1–200 ppm), using 10 ppm of polypropylene glycol 500 (PPG) as the internal standard. A 10 mM solution of α-Cyano-4-Hydroxycinnamic Acid (CHCA) in 50/50 acetonitrile/water with 0.1 % trifluoroacetic acid (TFA) was added to each sample at 1:1 v/v ratio, and 1 μL of the sample/matrix mixture was applied onto a Bruker AnchorChip target in triplicate and dried.

3.4. Carboxylic group density measurements

The carboxylic group density of the selective layer was measured using the ion elution method with Cu^+ as the binding agent. A 10 mM copper nitrate solution (ACS reagent, ≥99 %, Sigma) was first prepared in 1 wt. % HNO_3 and then diluted to 40 μM and 1 μM in deionized (DI) water to obtain solutions for copper binding and rinsing steps, respectively. The pH of each solution was adjusted to 7 using 0.1 M NaOH and 1 wt. % HNO_3. Membrane coupons were soaked in DI water for 24 hours, followed by immersion in 10 mL of the 40 μM copper nitrate solution for two consecutive 10-minute cycles to allow one-to-one binding between copper ions and ionized carboxyl groups. The coupons were then rinsed in 10 mL of the 1 μM copper nitrate solution for 7 min to remove unbound copper ions; this step was repeated four times to ensure effective binding. After each immersion, the membrane surface was gently blotted with Kimwipes to minimize solution carryover. Finally, the coupons were immersed in 5 mL of 1 wt. % HNO_3 for 30 min to protonate the carboxyl groups and elute the bound copper ions. The resulting copper ion concentration was measured using ICP-MS and used to calculate the carboxylic group density (Chen et al., 2017).

CRediT authorship contribution statement

Mohsen Pilevar: Writing – original draft, Investigation, Formal analysis, Data curation. **Hesam Jafarian:** Writing – original draft, Visualization, Investigation, Formal analysis. **Nima Behzadnia:** Methodology, Investigation, Formal analysis, Data curation. **Qiaoli Liang:** Writing – review & editing, Validation, Resources, Methodology, Data curation. **Sanam Etemadi Maleki:** Writing – original draft, Investigation, Data curation. **Sadegh Aghapour Aktij:** Writing – review & editing, Investigation, Formal analysis, Data curation. **Mohtada Sadrzadeh:** Writing – review & editing, Validation, Resources, Methodology. **Leigh Terry:** Writing – review & editing, Validation, Resources. **Mark Elliott:** Writing – review & editing, Validation, Supervision, Resources, Project administration, Funding acquisition, Conceptualization. **Mostafa Dadashi Firouzjaei:** Writing – review & editing, Visualization, Validation, Supervision, Software, Resources, Project administration, Methodology, Investigation, Data curation, Conceptualization.

Declaration of competing interest

The authors declare that they have no known competing financial interests or personal relationships that could have appeared to influence the work reported in this paper.

Acknowledgments

This research benefited greatly from funding provided by USDATAT-RWTS 00–69526, USEPA Cooperative Agreement MX-00D87019, The Richard Lounsbery Foundation, the Transforming Wastewater Infrastructure in the United States project of Columbia World Projects, and NSF EPSCoR Grant RII Track 4 (#2228903). USDA, NSF, or other agencies have not formally reviewed this paper, and the views expressed in this document are solely those of the authors and do not necessarily reflect those of the agencies.

Supplementary materials

Supplementary material associated with this article can be found, in the online version, at doi:10.1016/j.wroa.2025.100358.

Data availability

Data will be made available on request

References

Ahn, S.-K., et al., 2022. Adsorption mechanisms on perfluorooctanoic acid by FeCl3 modified granular activated carbon in aqueous solutions. Chemosphere 303, 134965.

Aktij, S.A., et al., 2023. High perm-selectivity and performance of tuned nanofiltration membranes by merging carbon nitride derivatives as interphase layer for efficient water treatment. J. Water Process Eng. 56, 104432.

Ang, W.S., Elimelech, M., 2007. Protein (BSA) fouling of reverse osmosis membranes: implications for wastewater reclamation. J. Memb. Sci. 296 (1–2), 83–92.

Boo, C., et al., 2018. High performance nanofiltration membrane for effective removal of perfluoroalkyl substances at high water recovery. Env. Sci. Technol 52 (13), 7279–7288.

Chang, E.T., et al., 2014. A critical review of perfluorooctanoate and perfluorooctanesulfonate exposure and cancer risk in humans. Crit. Rev. Toxicol. 44 (sup1), 1–81.

Chaudhary, M., et al., 2023. Efficient PFOA removal from drinking water by a dual-functional mixed-matrix-composite nanofiltration membrane. npj Clean Water 6 (1), 77.

Chen, C., et al., 2021. Photocatalytically reductive defluorination of perfluorooctanoic acid (PFOA) using Pt/La2Ti2O7 nanoplates: experimental and DFT assessment. J. Hazard. Mater 419, 126452.

Chen, D., et al., 2017. A facile method to quantify the carboxyl group areal density in the active layer of polyamide thin-film composite membranes. J. Memb. Sci. 534, 100–108.

Cheng, W., et al., 2019. Graphene oxide-functionalized membranes: the importance of nanosheet surface exposure for biofouling resistance. Env. Sci. Technol 54 (1), 517–526.

Cui, J., et al., 2022. Perfluorooctane sulfonate induces dysfunction of human umbilical vein endothelial cells via ferroptosis pathway. Toxics 10 (9), 503.

(EPA), U.S.E.P.A, 2024. The National Primary Drinking Water Regulations (NPDWR).

Fabrega, J., et al., 2011. Silver nanoparticles: behaviour and effects in the aquatic environment. Env. Int 37 (2), 517–531.

Firouzjaei, M.D., et al., 2018. Exploiting synergetic effects of graphene oxide and a silver-based metal–organic framework to enhance antifouling and anti-biofouling properties of thin-film nanocomposite membranes. ACS Appl. Mater. Interfaces 10 (49), 42967–42978.

Hopkins, Z.R., et al., 2018. Recently detected drinking water contaminants: GenX and other per-and polyfluoroalkyl ether acids. J.-Am. Water Works Assoc. 110 (7), 13–28.

Jafarian, H., et al., 2023. Synthesis of heterogeneous metal organic framework-graphene oxide nanocomposite membranes for water treatment. Chem. Eng. J. 455, 140851.

Kebede, M.M., et al., 2024. Mapping per-and polyfluoroalkyl substance footprint from cosmetics and carpets across the continental United States. ACS ES&T Water 4 (9), 3882–3892.

Khorshidi, B., et al., 2015. Thin film composite polyamide membranes: parametric study on the influence of synthesis conditions. RSC Adv. 5 (68), 54985–54997.

Kucharzyk, K.H., et al., 2017. Novel treatment technologies for PFAS compounds: a critical review. J. Env. Manage 204, 757–764.

Léniz-Pizarro, F., et al., 2022. Dual-functional nanofiltration and adsorptive membranes for PFAS and organics separation from water. ACS ES&T Water 2 (5), 863–872.

Li, M., et al., 2021. Removal mechanisms of perfluorinated compounds (PFCs) by nanofiltration: roles of membrane-contaminant interactions. Chem. Eng. J. 406, 126814.

Liu, Y.-L., Sun, M., 2021. Ion exchange removal and resin regeneration to treat per-and polyfluoroalkyl ether acids and other emerging PFAS in drinking water. Water Res. 207, 117781.

Liu, Z., et al., 2022. Thin-film composite nanofiltration membranes with poly (amidoxime) as organic interlayer for effective desalination. J. Environ. Chem. Eng. 10 (1), 107015.

Longendyke, G.K., Katel, S., Wang, Y., 2022. PFAS fate and destruction mechanisms during thermal treatment: a comprehensive review. Environ. Sci. Process. Impacts 24 (2), 196–208.

Mazani, M., et al., 2019. Cu-BTC metal– organic framework modified membranes for landfill leachate treatment. Water 12 (1), 91.

Melzer, D., et al., 2010. Association between serum perfluorooctanoic acid (PFOA) and thyroid disease in the US National Health and Nutrition Examination Survey. Env. Health Perspect 118 (5), 686–692.

Merino, N., et al., 2016. Degradation and removal methods for perfluoroalkyl and polyfluoroalkyl substances in water. Env. Eng. Sci 33 (9), 615–649.

Mohammad, A.W., et al., 2015. Nanofiltration membranes review: recent advances and future prospects. Desalination 356, 226–254.

Nejad, S.M., et al., 2022. Loose nanofiltration membranes functionalized with in situ-synthesized metal organic framework for water treatment. Mater. Today Chem. 24, 100909.

Organization, W.H., 2022. Guidelines For Drinking-Water quality: Incorporating the First and Second Addenda. World Health Organization.

Park, S.-H., et al., 2016. Direct incorporation of silver nanoparticles onto thin-film composite membranes via arc plasma deposition for enhanced antibacterial and permeation performance. J. Memb. Sci. 513, 226–235.

Pilevar, M., et al., 2024. Analysis of metal–organic framework and polyamide interfaces in membranes for water treatment and antibacterial applications. Small Methods, 2401566.

Sadrzadeh, M., Bhattacharjee, S., 2013. Rational design of phase inversion membranes by tailoring thermodynamics and kinetics of casting solution using polymer additives. J. Memb. Sci 441, 31–44.

Shah, S.S.A., et al., 2024. Recent trends in wastewater treatment by using metal-organic frameworks (MOFs) and their composites: a critical view-point. Chemosphere 349, 140729.

Shao, S., et al., 2022. Nanofiltration membranes with crumpled polyamide films: a critical review on mechanisms, performances, and environmental applications. Env. Sci. Technol 56 (18), 12811–12827.

Steenland, K., et al., 2013. Ulcerative colitis and perfluorooctanoic acid (PFOA) in a highly exposed population of community residents and workers in the mid-Ohio valley. Env. Health Perspect. 121 (8), 900–905.

Sun, L., et al., 2025. Efficiency and mechanisms of combined persulfate and nanofiltration for the removal of typical perfluorinated compounds. Environ. Sci.: Water Res. Technol.

Sun, R., et al., 2024. New insights into thermal degradation products of long-chain per-and polyfluoroalkyl substances (PFAS) and their mineralization enhancement using additives. Env. Sci. Technol.

Tang, W., et al., 2022. Preparation of hollow-fiber nanofiltration membranes of high performance for effective removal of PFOA and high resistance to BSA fouling. J. Environ. Sci. 122, 14–24.

Teng, B., et al., 2024. Progress on the removal of PFAS contamination in water by different forms of iron-modified biochar. Chemosphere 369, 143844.

Tian, R., et al., 2024. Nanofiltration membrane functionalization with enhanced hardness cation removal using a mono-component interlayer. Desalination 586, 117870.

Urper-Bayram, G.M., et al., 2020. Comparative impact of SiO2 and TiO2 nanofillers on the performance of thin-film nanocomposite membranes. J. Appl. Polym. Sci. 137 (44), 49382.

Wang, Y., et al., 2020. Removal of emerging wastewater organic contaminants by polyelectrolyte multilayer nanofiltration membranes with tailored selectivity. ACS ES&T Eng. 1 (3), 404–414.

Wolkeba, F.T., et al., 2024. Indicator metrics and temporal aggregations introduce ambiguities in water scarcity estimates. Sci. Rep. 14 (1), 15182.

Woodard, S., Berry, J., Newman, B., 2017. Ion exchange resin for PFAS removal and pilot test comparison to GAC. Remediat. J. 27 (3), 19–27.

Xie, Y., Sherwood, P., 1992. P55X pitch-based carbon fiber by core level and valence band XPS. Surf. Sci. Spectra 1 (2), 192–197.

Xiong, J., et al., 2021. The rejection of perfluoroalkyl substances by nanofiltration and reverse osmosis: influencing factors and combination processes. Environ. Sci. Water Res. Technol. 7 (11), 1928–1943.

Zango, Z.U., et al., 2023. A review on superior advanced oxidation and photocatalytic degradation techniques for perfluorooctanoic acid (PFOA) elimination from wastewater. Env. Res 221, 115326.

Zhang, L., et al., 2024. Persulfate activation for efficient remediation of perfluorooctanoic acid (PFOA) and perfluorooctane sulfonic acid (PFOS) in water: mechanisms, removal efficiency, and future prospects. J. Environ. Chem. Eng. 12 (1), 111422.

Zirehpour, A., et al., 2016. The impact of MOF feasibility to improve the desalination performance and antifouling properties of FO membranes. RSC Adv. 6 (74), 70174–70185.